Electronic Supplementary Information (ESI)

Facile Synthesis of Fe_2P/Co Embedded Trifunctional Electrocatalyst for High-Performance Anion Exchange Membrane Fuel Cells, Rechargeable Zn-Air Batteries and Overall Water Splitting

Yang Bai,[#] Yaqin Wang,[#] Zelong Qiao,[#] Yongping Yang, Luanjie Deng, Chuanjie Li, Xiudong Chen, Shitao Wang,* Yan Huang,* Xianren Zhang and Dapeng Cao*

State Key Laboratory of Organic-Inorganic Composites, Beijing University of Chemical Technology, Beijing 100029 (P. R. China)

*Corresponding authors: stwang@buct.edu.cn; huangyan@buct.edu.cn; caodp@mail.buct.edu.cn.

[#] These authors contributed equally to this work

Experimental section

Materials

All chemicals were from commercial and used without further purification. Zinc nitrate hexahydrate (Zn $(NO_3)_2 \cdot 6H_2O$, 98%) and Pt/C catalysts (20 wt% Pt loading on an activated carbon support) were obtained from Alfa Aesar. IrO_2 and 2-methylimidazole (98%) were purchased from Aladdin. Cobalt nitrate hexahydrate (Co $(NO_3)_2 \cdot 6H_2O$, 99%) and 1, 1'-Bis (diphenylphosphino) ferrocene (97%) were purchased from Macklin.

Synthesis of DPPF@ZnCo-ZIF

Firstly, 0.6158 g 2-methylimidazole was dissolved in 15 mL methanol by ultrasonic treatment for 2 min to prepare a homogeneous solution A. Secondly, 0.4462 g Zn $(NO_3)_2 \cdot 6H_2O$, 0.3274 g $Co(NO_3)_2 \cdot 6H_2O$ and 0.2079 g DPPF were dissolved in 30 mL methanol with well stirring for 60min to prepare solution B. Then, solution A was quickly added to solution B and stirred strongly for 1.5 h at room temperature. Next, the mixture solution was transferred to a 100 mL stainless steel autoclave and heated at 120 ° C for 4 h. The prepared products were collected through the centrifugal process and washed with methanol for several times. Finally, they were dried in vacuum at 70 °C for 12 h to obtain DPPF@ZnCo-ZIF. ZnCo-ZIF and DPPF@Zn-ZIF were also synthesized via similar procedure without adding DPPF or Co $(NO_3)_2 \cdot 6H_2O$, respectively.

Synthesis of Fe_2P/Co@NPC

The resulting powder DPPF@ZnCo-ZIF, ZnCo-ZIF and DPPF@Zn-ZIF were calcined under Ar at 950 °C (ramp rate: 5 °C min^{-1}) for 3 h separately and then cooled to room temperature. The Fe_2P/Co@NPC, Co@NC and Fe_2P@NPC were collected without further treatment. To determine the optimum conditions for the formation of Fe_2P/Co@NPC catalysts, different pyrolysis temperatures

(850, 950, 1050 °C) were also examined denoted as Fe_2P/Co@NPC -X (X =850,950,1050). The Fe_2P/Co@NPC mentioned below refers to the sample synthesized with the temperature at 950 °C in particular.

Structural characterization of the samples

SEM and TEM images of the samples were received by HITACHI S-4800 and TECNAI G2 F20 microscopes, respectively. PXRD were performed on a D8 ADVANCE X-ray diffractometer (Cu Kα radiation as source). The pore structure was investigated by N_2 adsorption-desorption measurements on an ASAP 2460 instrument. XPS measurements were conducted on the Thermo Fisher ESCALAB 250 with an A1 Kα X-ray source. In order to determine the element contents, ICP measurements were conducted on Inductively Coupled Plasma Optical Emission Spectrometer (ICP-OES). Raman spectra were recorded on a LabRam HR Evolution, using 514 nm as laser.

Electrochemical measurements

The Electrochemical performances of ORR, OER and HER were recorded by Electrochemical Workstation (CHI 760E, Shanghai Chenhua Instrument Corporation, China). All electrochemical measurements were made on a typical three-electrode system. Platinum mesh was used as counter electrode for ORR test, graphite rod for OER and HER test. The saturated calomel electrode is used as a reference electrode. All the potential is converted to a reversible hydrogen electrode. For ORR, the LSV curves were obtained in a 0.1 M KOH solution saturated with O_2 at a scan rate of 5 $mV \cdot s^{-1}$ and a rotation speed of 1600 rpm in the potential range of 0.1 to -1 V. The electron transfer number (n) and the yield of H_2O_2 are obtained from the following equation through RRDE:

$$n = 4\frac{I_D}{\frac{I_R}{N} + I_D}$$

$$H_2O_2\% = 200\frac{I_R/N}{\frac{I_R}{N}+I_D}$$

where I_D is disk current，I_R is ring current, and N is the current collection efficiency of the Pt ring, N = 0.37.[1]

The electron transfer number (n) and kinetic current density (J_k) can also be calculated based on the Koutecky-Levich (K-L) equation:

$$\frac{1}{J}=\frac{1}{J_K}+\frac{1}{J_L}=\frac{1}{B\omega^{\frac{1}{2}}}+\frac{1}{J_K}$$

$$B = 0.62nFC_0D_0^{\frac{2}{3}}V^{-\frac{1}{6}}$$

Where J is the measured current density, J_K and J_L are the kinetic and limiting current density respectively, ω is the angular velocity of the disk, n is the number of electron transfers, F is the Faraday constant (96485 C·mol^{-1}), and C_0 is the concentration of O_2(1.2×10^{-6} mol·cm^{-3}), D_0 is the diffusion coefficient of O_2 in 0.1 M KOH (1.9×10^{-5} cm^2·s^{-1}), and V is the kinematic viscosity of the electrolyte (0.01 cm^2·s^{-1}).[2] To eliminate the error, the oxygen reduction current (J) the oxygen reduction current is calculated as the current measured in saturated oxygen minus saturated nitrogen.

The 1 M KOH solution was used as the electrolyte for OER and HER tests. All LSV curves are obtained by IR compensation. The CV curves at different scan rates are also measured to determine the electrochemical double layer capacitance (C_{dl}), and then ESCA can be calculated based on the C_{dl} value.

The synthesized Fe_2P/Co@NPC were applied as the cathode catalyst with the loading of 1 mg cm^{-2}. PtRu/C (40 wt% Pt and 20 wt% Ru on Vulcan XC-72, Johnson Matthey) was used as the anode catalyst with the loading of 0.4 mg_{PtRu} cm^{-2}. The catalyst ink was prepared by ultrasonically dispersing the catalysts and PAP-TP-100 (the hydroxide exchange membrane and ionomer, 5 wt% in ethanol) into

water and isopropanol (1:25 v/v) for 2.0 h. Then the catalyst ink was sprayed onto both sides of PAP-TP-85 membrane (15 μm) to fabricate a catalyst-coated membrane (CCM) with the electrode area of 5 cm^{-2}. All CCMs were immersed into 3 M KOH solution for 4.0 h (exchange the solution every 2.0 h) and then rinsed thoroughly with deionized water until the pH of the residual water was neutral. The obtained CCM was assembled with a fluorinated ethylene propylene (FEP) gasket, a GDL (SGL 29 BC), a graphite bipolar plate with 5 cm^2 flow field (Electro Chem) and a metal current collector for each side to complete the full HEMFC. The H_2-O_2 fuel cell were tested (Scribner 850e) under galvanic mode using humidified H_2 and O_2. The cell temperature was set to 80 ºC, and the flow rate of both H_2 and O_2 gas was 1.0 and 1.5 L min^{-1} with 2.5 bar backpressure.

We assembled a self-made Zn-air battery, in which 6 M KOH and 0.2 M ZnO were served as electrolyte, zinc piece and Fe_2P/Co@NPC-loaded carbon paper (1 mg cm^{-2}) used as the anode and air cathode, respectively. The stability of Fe_2P/Co@NPC was evaluated using a rechargeable zinc air battery at a current density of 5 mA cm^{-2}. For comparison, a Zn-air battery based on Pt/C-IrO_2 was also assembled (using a mixture of Pt/C and IrO_2 as an electrocatalyst with a mass ratio of 1:1). In order to test the overall water-splitting activity, two identical Fe_2P/Co@NPC electrodes coated on carbon paper were assembled into a full electrolyzer configuration. The catalyst loading was 1 mg·cm^{-2} in 1M KOH solution.

Working electrode preparations

In short, a 5mg sample was dispersed in a 1mL solution containing 600 μL anhydrous ethanol, 400 μL water, and 50 μL Nafion (5 wt%) to prepare homogeneous catalytic ink and then treated with

ultrasound for 1 h. Then the obtained homogeneous catalyst inks 15 μL were dropped onto RDE (0.19625 cm^2) and then dried at room temperature to afford a mass loading of about 0.364 mg cm^{-2}. Commercial platinum carbon (20 wt%) and IrO_2 catalyst inks were prepared using the same process for comparison.

DFT calculation details.

DFT calculations were performed through the projector augmented wave (PAW) method by using the Vienna ab initio simulation package (VASP). The Generalized gradient approximation (GGA) method with the Perdew-Burke-Ernzerhof (PBE) was adopted as the exchange-correlation functional. The kinetic cutoff energy was set to 450 eV. The k-mesh in Brillouin zones was determined based on Monkhorst–Pack kpoint grids. The calculation uses gamma-centered k-points 1×3×1 for Fe_2P(111)-Co(111) heterojunction, 6×5×1 for Co(111), 5×5×1 for Fe_2P(111), zero damping DFT-D3 method of Grimme, and the convergence tolerance for the residual force and energy on each atom during structure relaxation were set to 0.02 $eVÅ^{-1}$ and 10^{-5} eV. The spin was constrained for all the systems with unpaired electrons. VASP-sol package[3] is used to simulate the solution environment, where the over dielectric constant (εr) is set to 80[4, 5]. The z-direction is set to 20 Å, which is to avoid steric hindrance and interaction due to periodicity. The optimization of the unit cell parameters is carried out by the method of fixing the lattice vector (modify constr_cell_relax.F file in VASP and recompile), the cell parameters are obtained as 30.000×6.758×20.000, a=b=c=90° for Fe_2P(111)-Co(111), 4.209×4.872×20.000, a=b=c=90 º for Co(111), and 6.438×6.439×20.000, a=b=90 º, c=94.802 º for Fe_2P (111). The free energy diagrams were estimated as follow to illustrate the activity of ORR [6, 7]:

$$\Delta G = \Delta E + \Delta ZPE - T\Delta S + \Delta G_U + \Delta G_{PH}$$

$$\varphi = G_{abslab} - G_{slab}$$

Where ΔE is the reaction energy of reactant and product molecules adsorbed on catalyst surface based on the DFT calculations; ΔZPE and ΔS are the change of zero-point energy and entropy, T is the temperature (here, 298.15 K is selected). The bias effect on the free energy is taken into account by ΔGU=−neU, where U is the electrode applied potential relative to RHE as mentioned above, e is the elementary charge transferred and n is the number of proton-electron pairs transferred. ΔGPH is the correction of the H+ free energy and depends on the reaction. In our work, the U is considered as 0 V, PH is 0, ΔZPE and ΔS are considered as G_K (calculated by VASP-kit code [8]), T is 298.15K. So we can get the following formula.

$$\Delta G = \Delta E + G_K$$

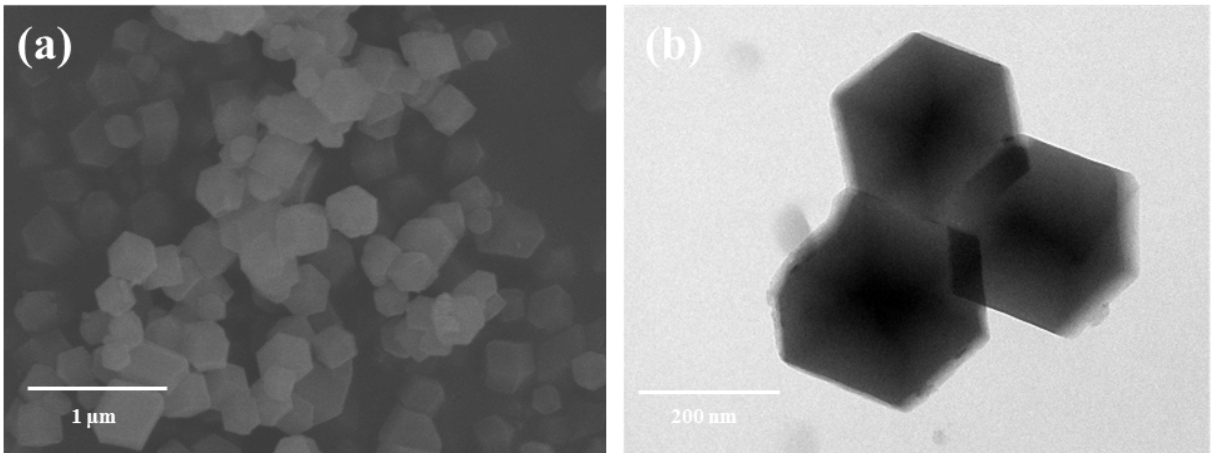

Figure S1. a) SEM image, b) TEM image of DPPF@ZnCo-ZIF.

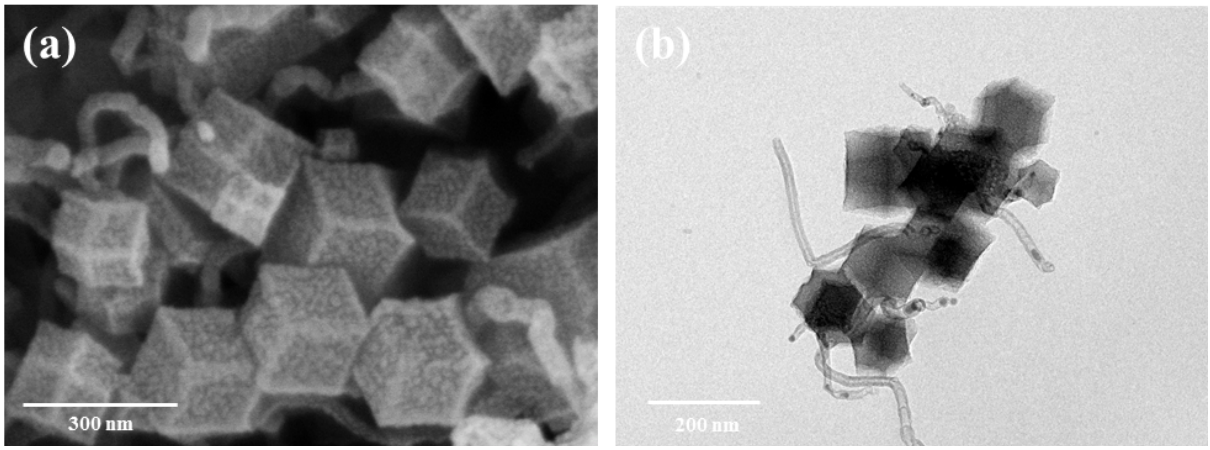

Figure S2. a) SEM image, b) TEM image of Co@NC.

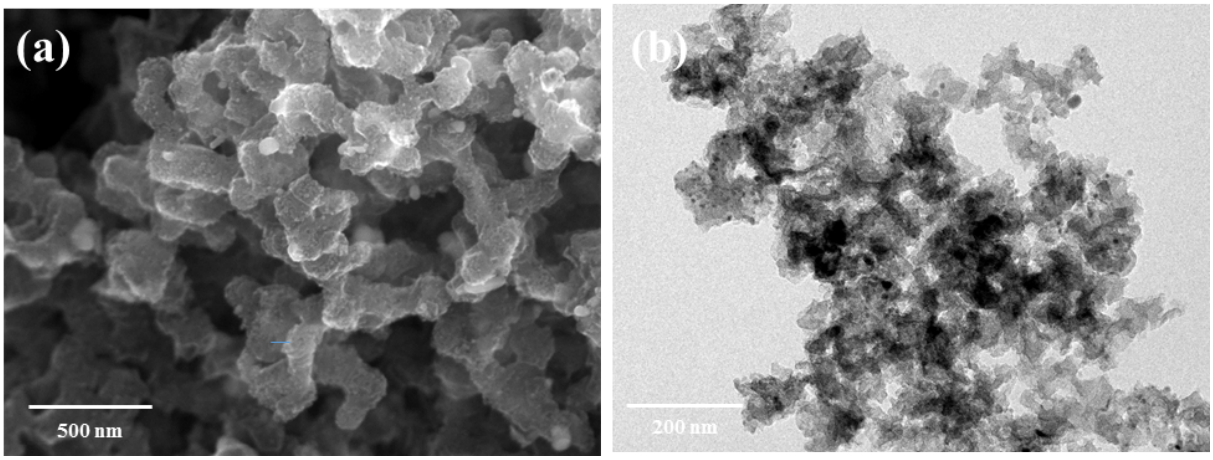

Figure S3. a) SEM image, b) TEM image of Fe_2P@NPC.

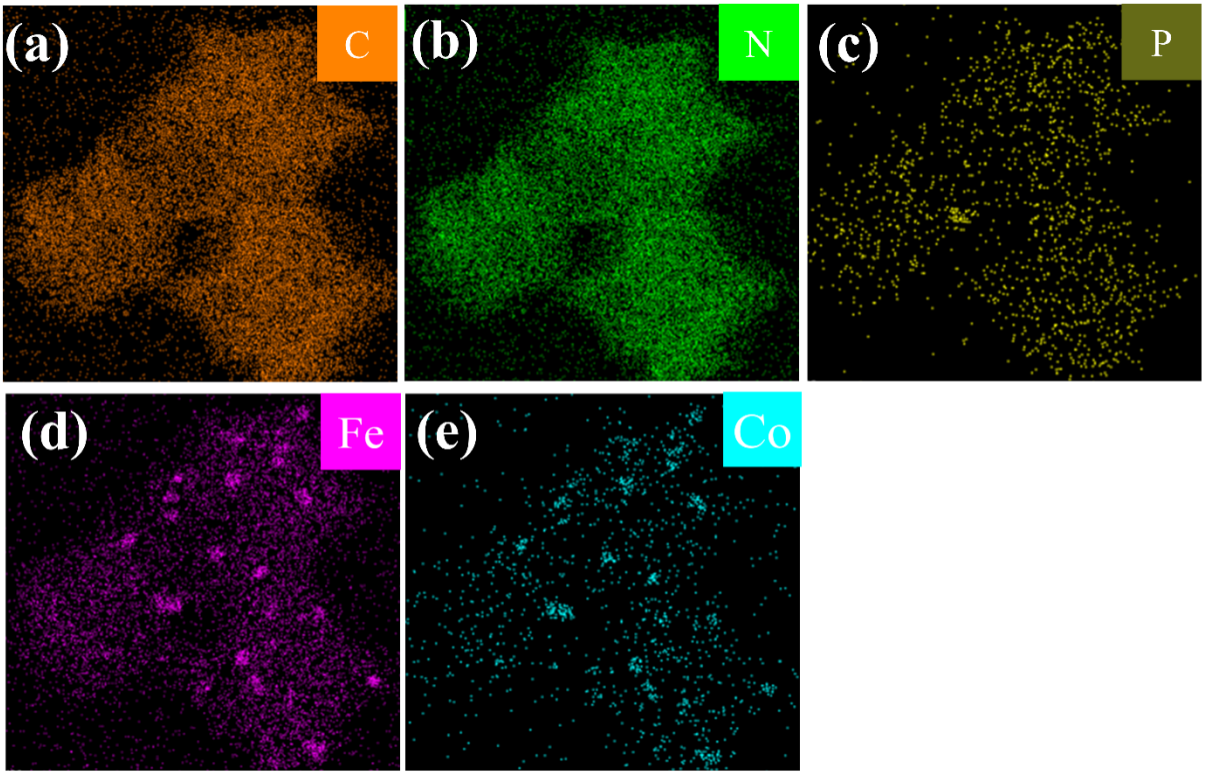

Figure S4. a-e) Elemental mapping of Fe_2P/Co@NPC.

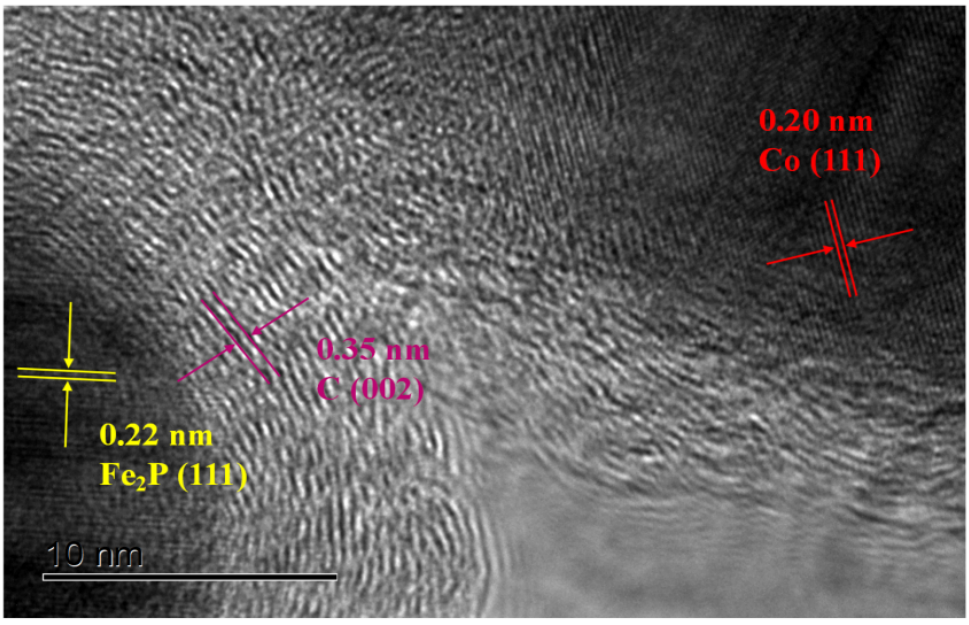

.

Figure S5. TEM image of Fe_2P/Co@NPC.

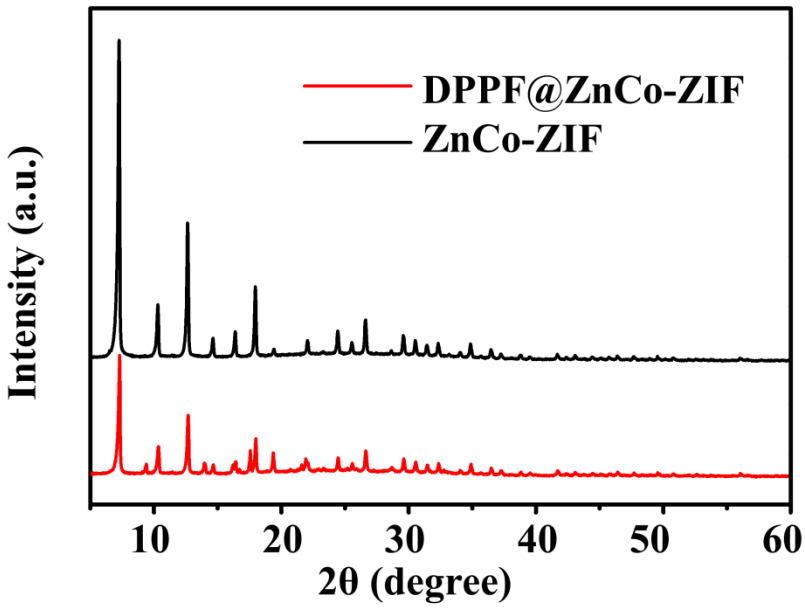

Figure S6. XRD pattern of DPPF@ZnCo-ZIF and ZnCo-ZIF.

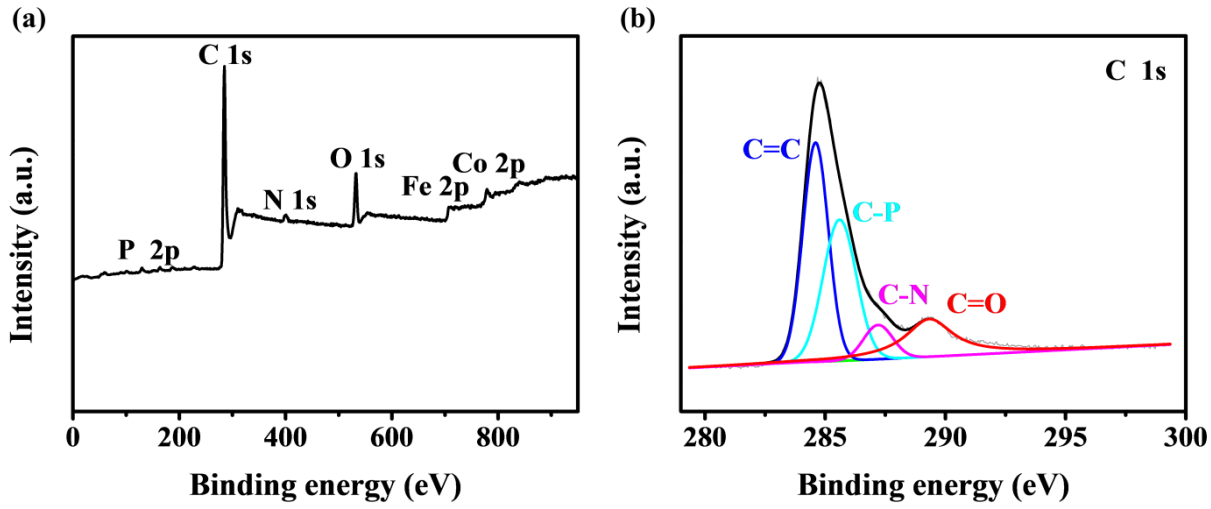

Figure S7. a) XPS survey spectrum (the inset table is surface atomic weight percentages). b) High-resolution XPS spectrum of C 1s of Fe_2P/Co@NPC.

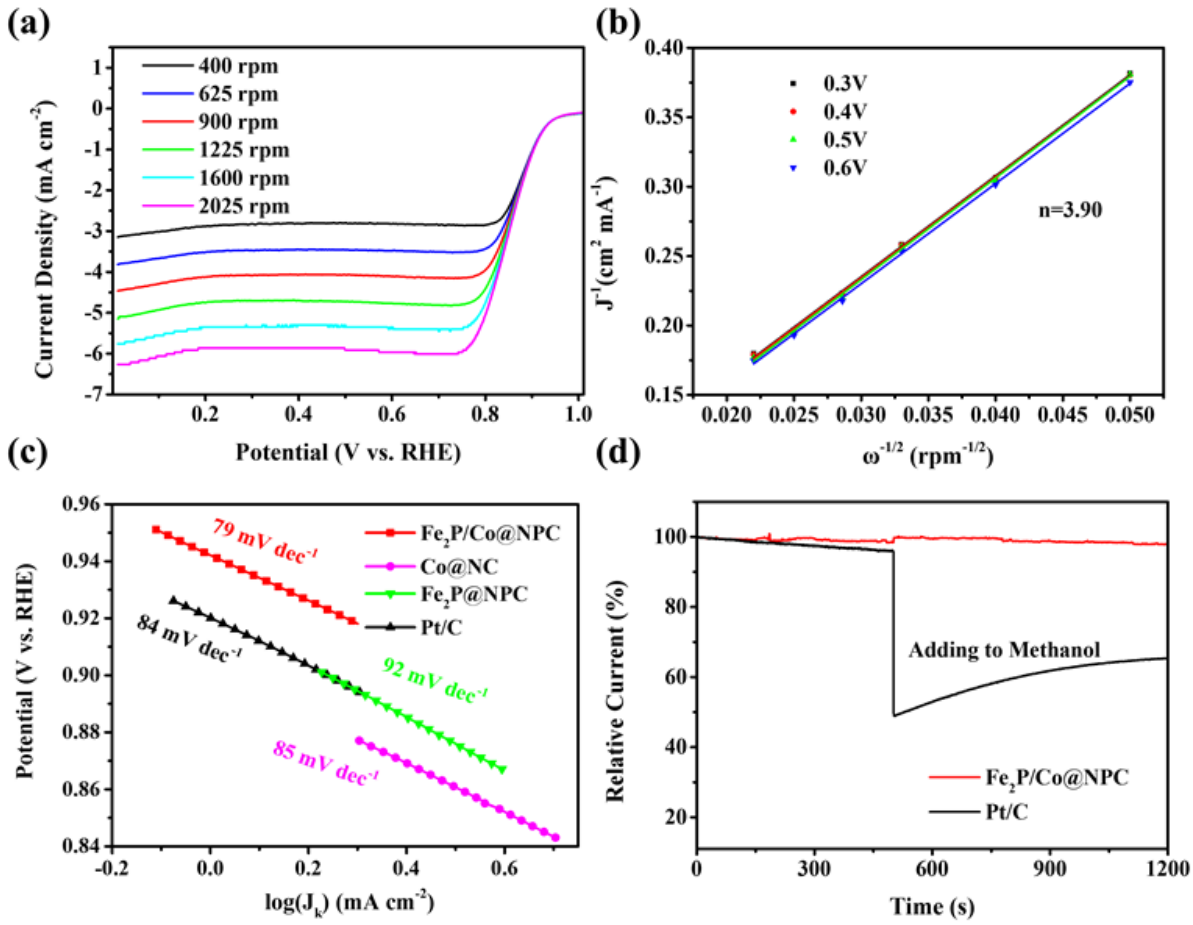

Figure S8. a) LSV curves of Fe_2P/Co@NPC sample at different rotation speed. b) K-L plots of Fe_2P/Co@NPC at different potentials. c) Tafel plot of Fe_2P/Co@NPC, Co@NC, Fe_2P@NPC and Pt/C. d) Chronoamperometric response of Fe_2P/Co@NPC and Pt/C with methanol added at 500 s.

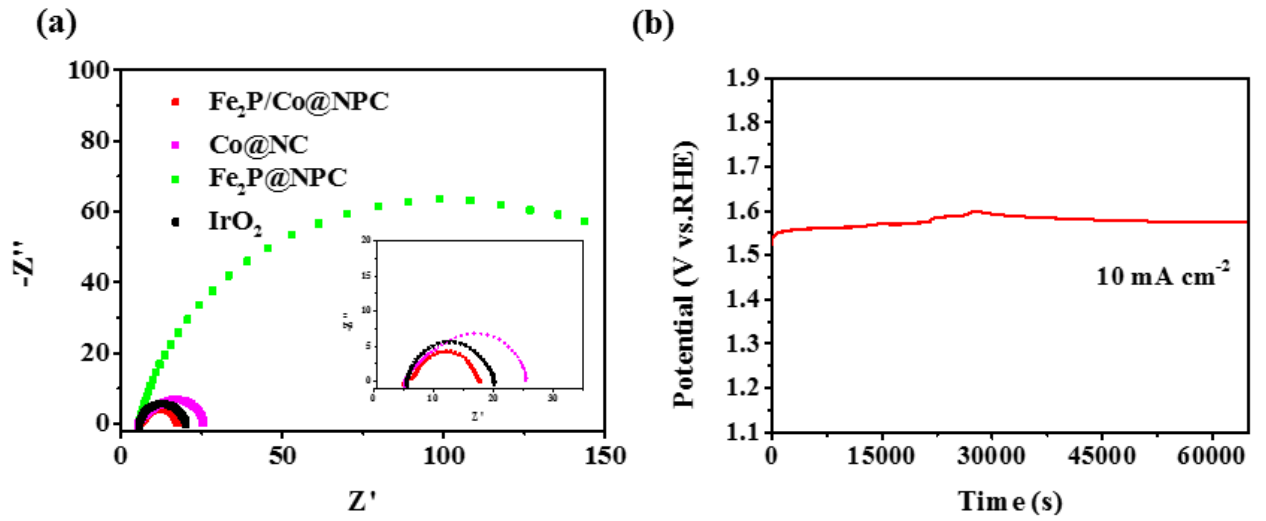

Figure S9. a) Nyquist plots for Fe_2P/Co@NPC, Co@NC, Fe_2P@NPC and IrO_2 during OER. b) Chronoamperometric responses of Fe_2P/Co@NPC in 1 M KOH at a current density of 10 mA cm^{-2} in OER.

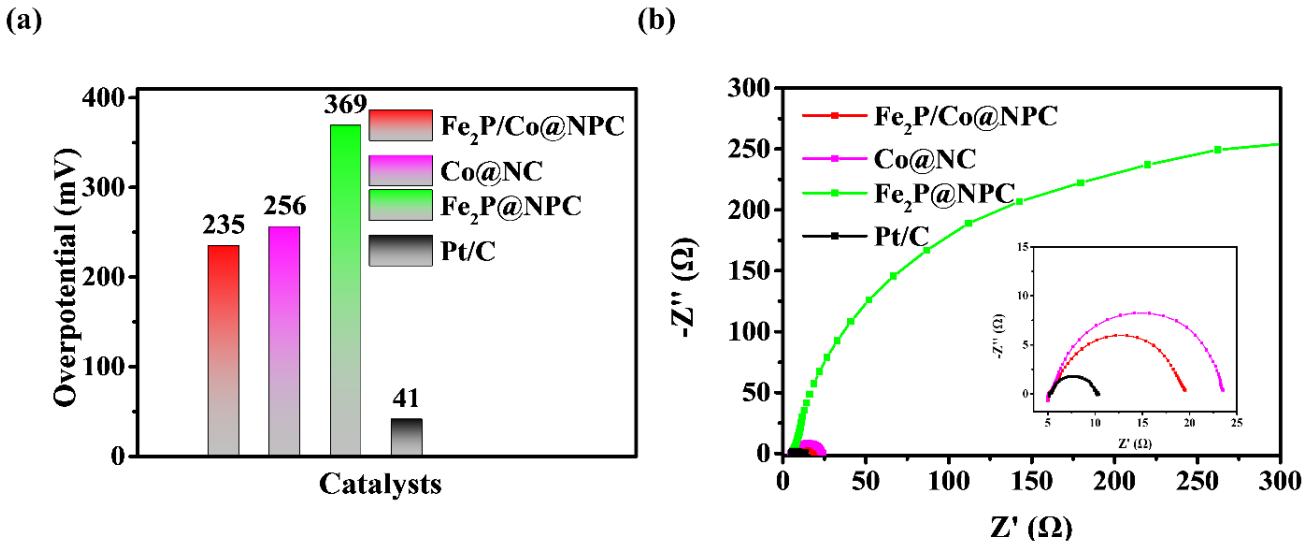

Figure S10. a) Comparison of the overpotential required at 10 mA cm^{-2} among Fe_2P/Co@NPC in HER. b) Nyquist plots for Fe_2P/Co@NPC, Co@NC, Fe_2P@NPC and Pt/C during HER.

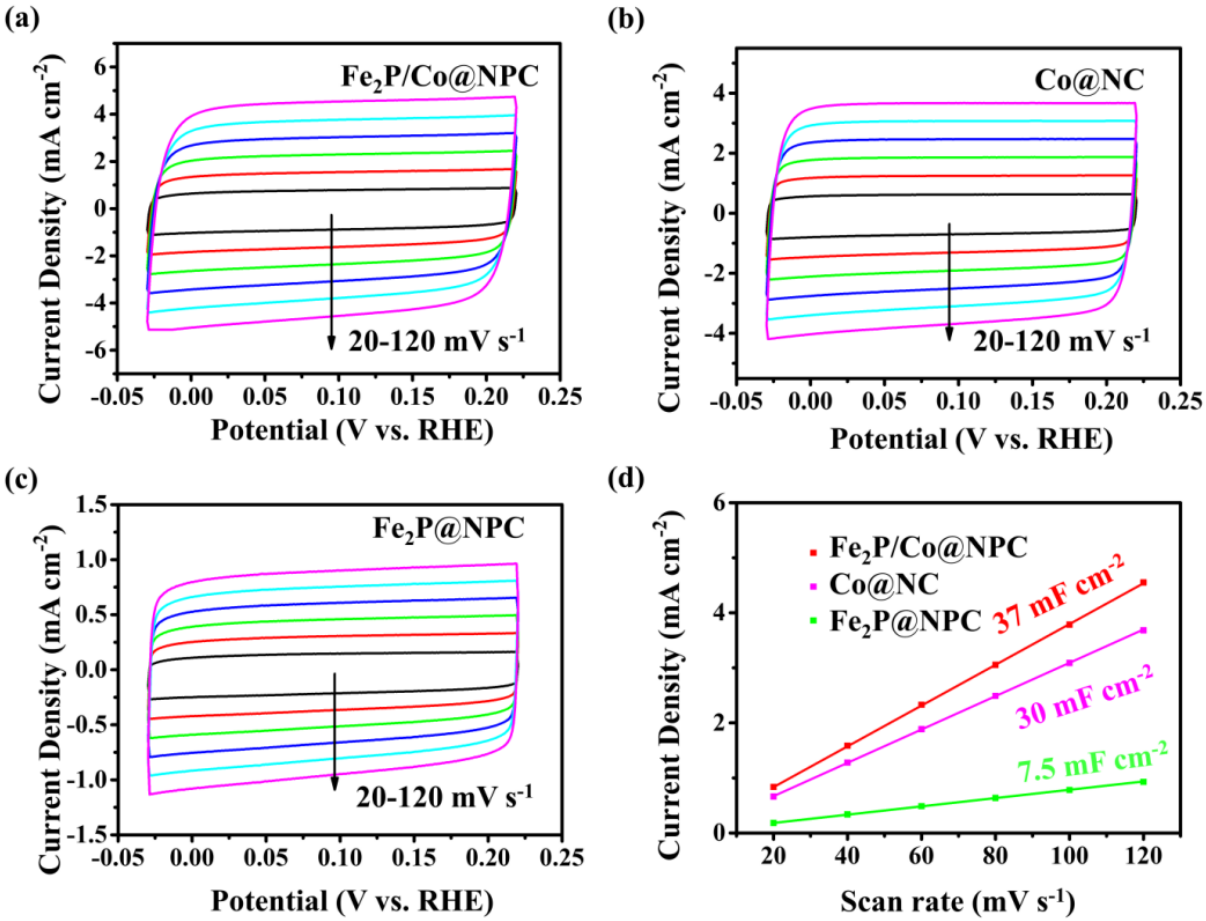

Figure S11. CV curves of a) Fe_2P/Co@NPC, b) Co@NC, c) Fe_2P@NPC in 1 M KOH electrolyte for HER. d) Current density versus scan rate for Fe_2P/Co@NPC, Co@NC and Fe_2P@NPC.

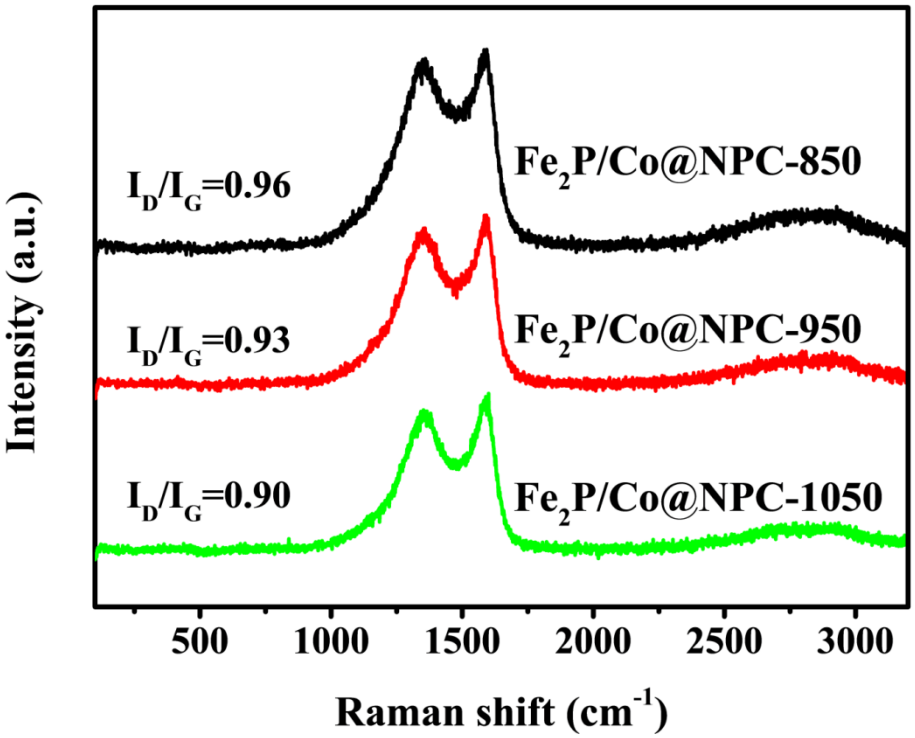

Figure S12. Raman spectra of Fe_2P/Co@NPCs at different pyrolysis temperature.

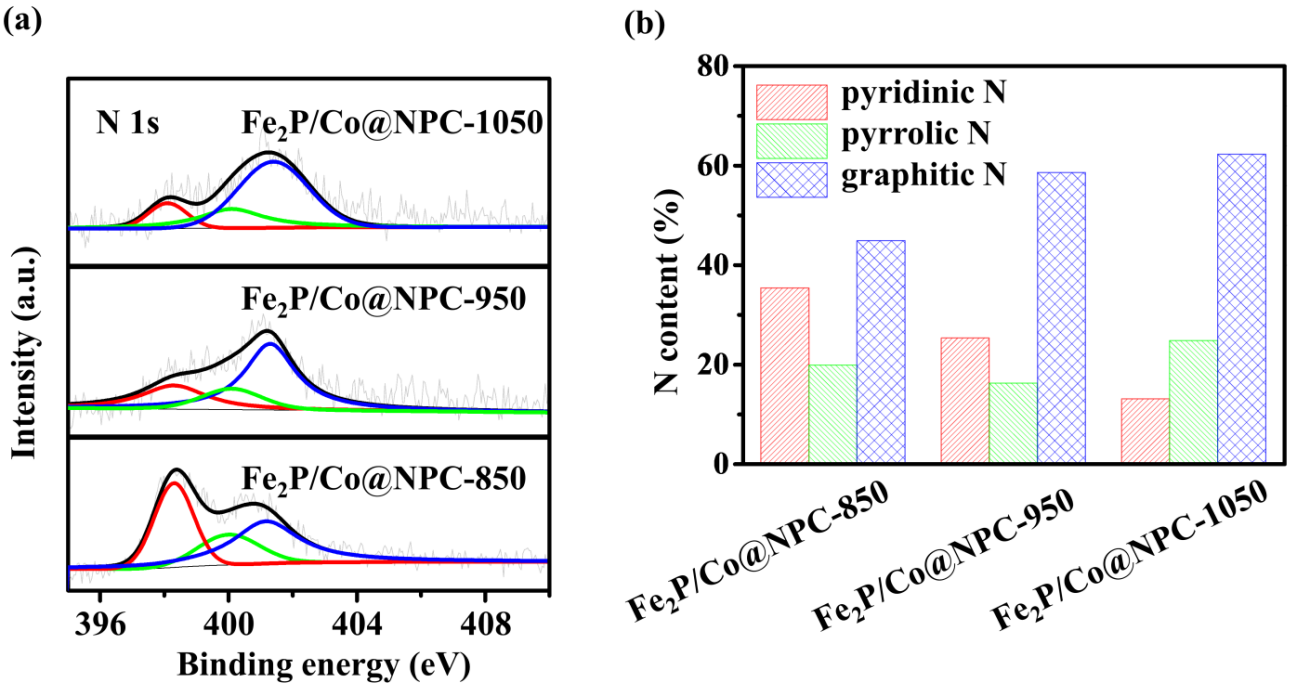

Figure S13. a) High-resolution XPS spectrum of N 1s for Fe_2P/Co@NPCs at different pyrolysis temperature. b) The contents of various doped N.

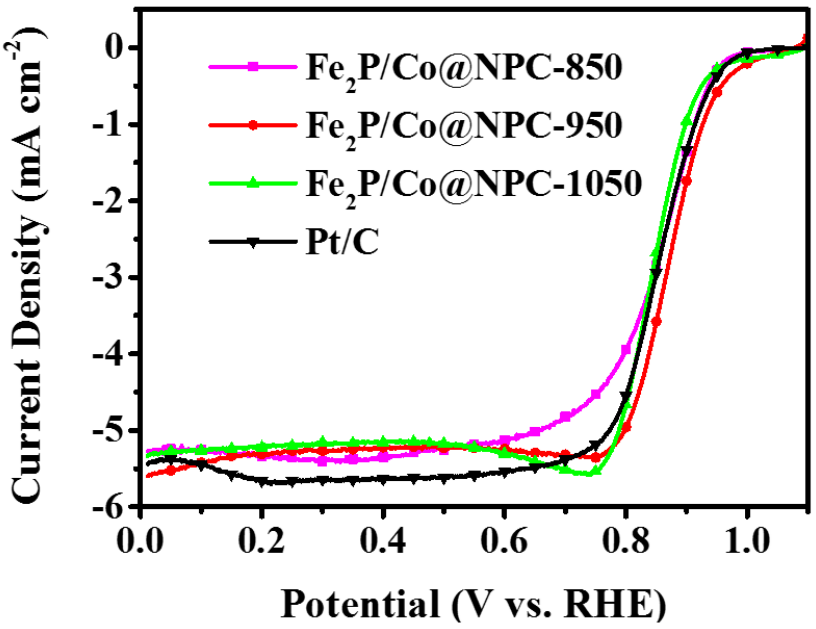

Figure S14. a) ORR polarization curves of Fe_2P/Co@NPCs at different pyrolysis temperature and Pt/C.

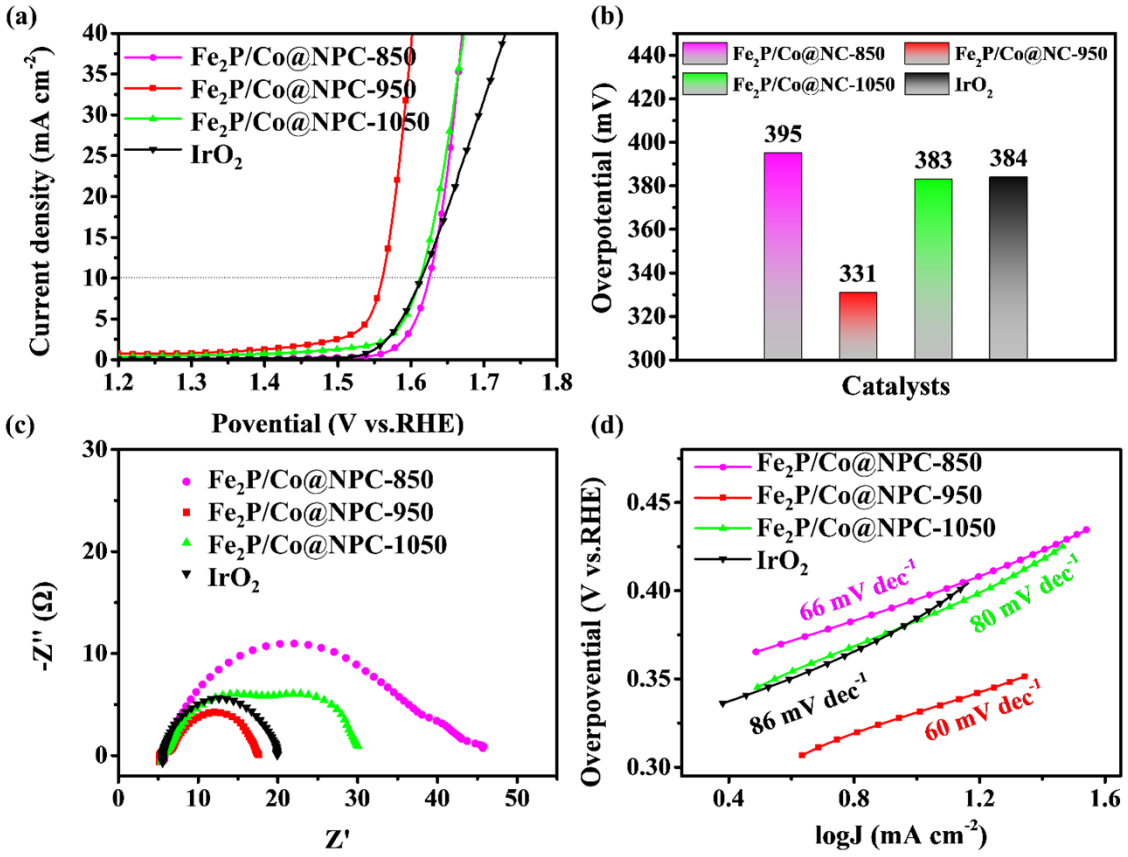

Figure S15. a) OER polarization curves, b) comparison of the overpotential required at 10 mA cm^{-2}, c) Nyquist plots, d) Tafel plot of Fe_2P/Co@NPCs at different pyrolysis temperature and IrO_2 in 1 M KOH.

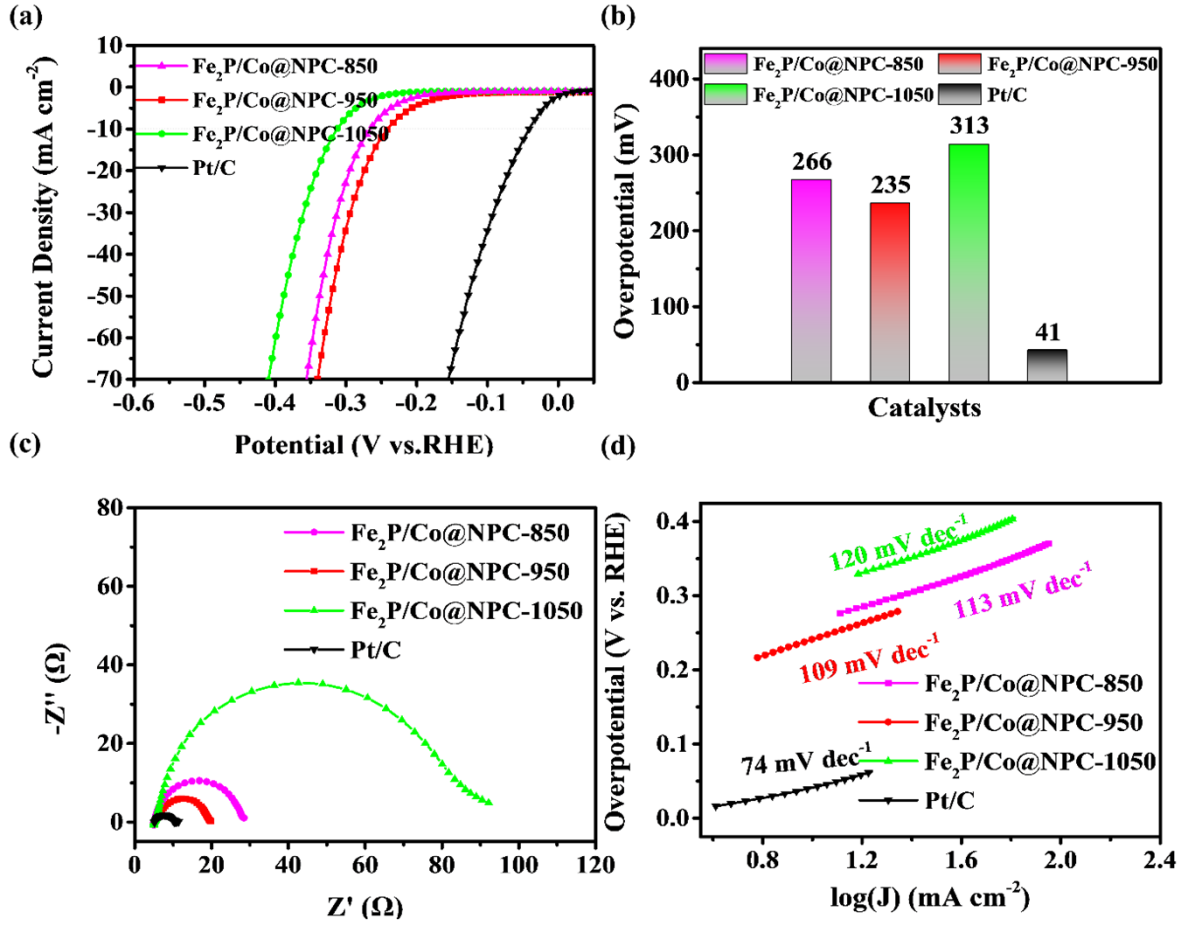

Figure S16. a) HER polarization curves, b) comparison of the overpotential required at 10 mA cm^{-2}, c) Nyquist plots, d) Tafel plot of Fe_2P/Co@NPCs at different pyrolysis temperature and Pt/C in 1 M KOH.

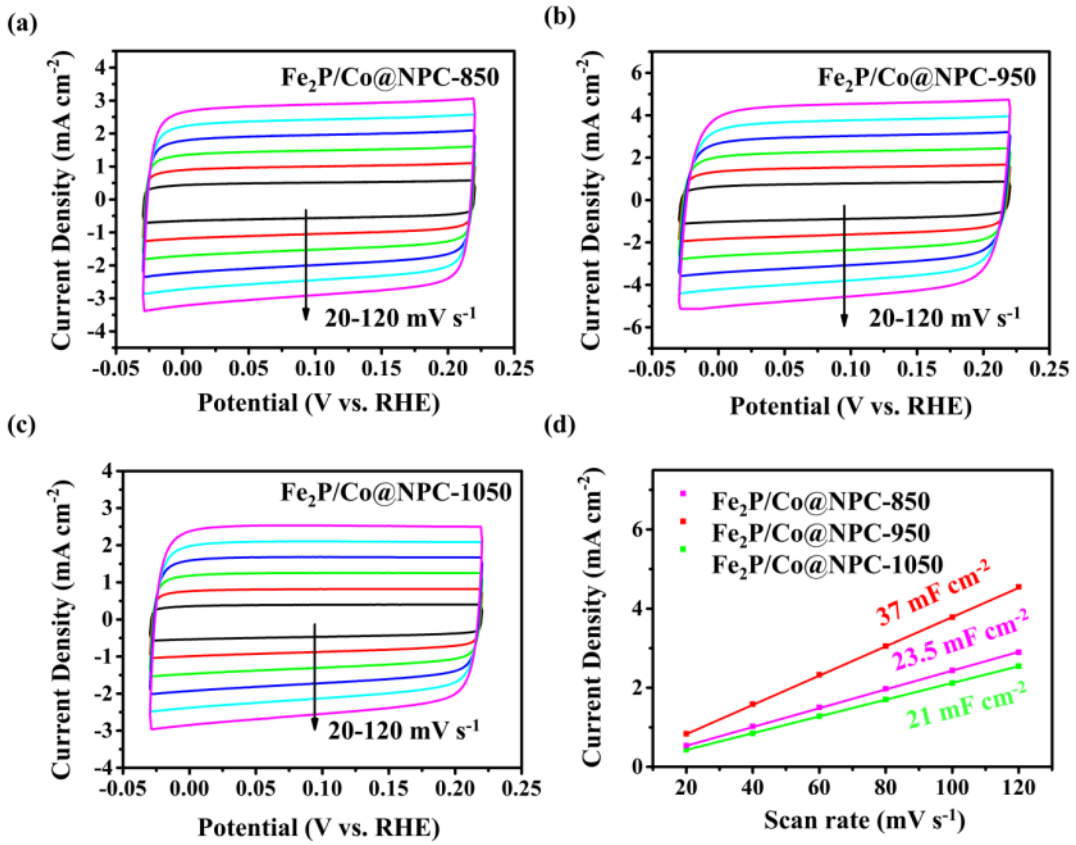

Figure S17. CV curves of a) Fe_2P/Co@NPC-850, b) Fe_2P/Co@NPC-950, c) Fe_2P/Co@NPC-1050 in 1 M KOH electrolyte for HER. d) Current density versus scan rate for Fe_2P/Co@NPCs at different pyrolysis temperature.

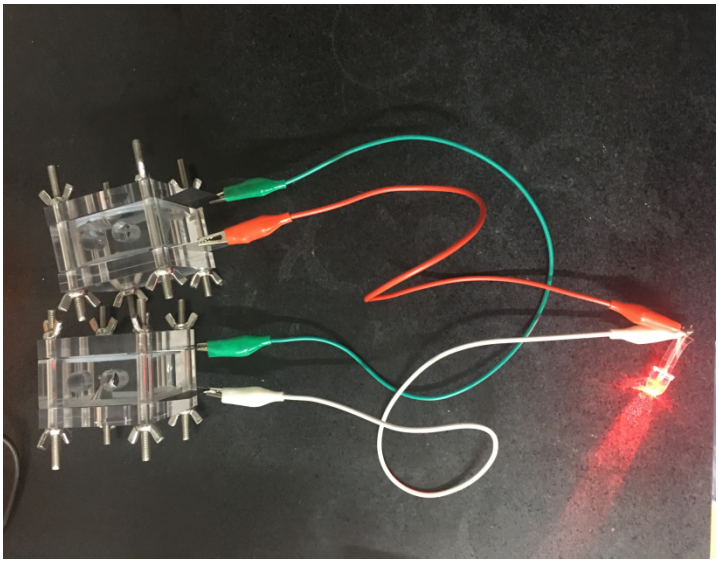

Figure S18. LED powered by two Zn–air batteries with the Fe_2P/Co@NPC as air-cathode connected in series.

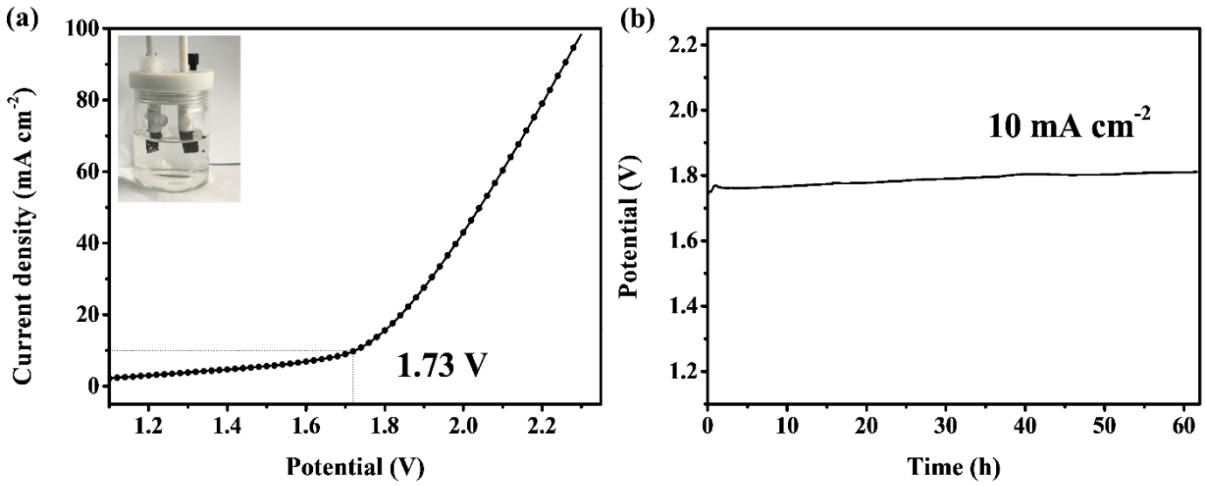

Figure S19. a) Polarization curves for overall water splitting (inset shows the photograph of a water electrolyzer). b) Chronoamperometric response curves for the water splitting device.

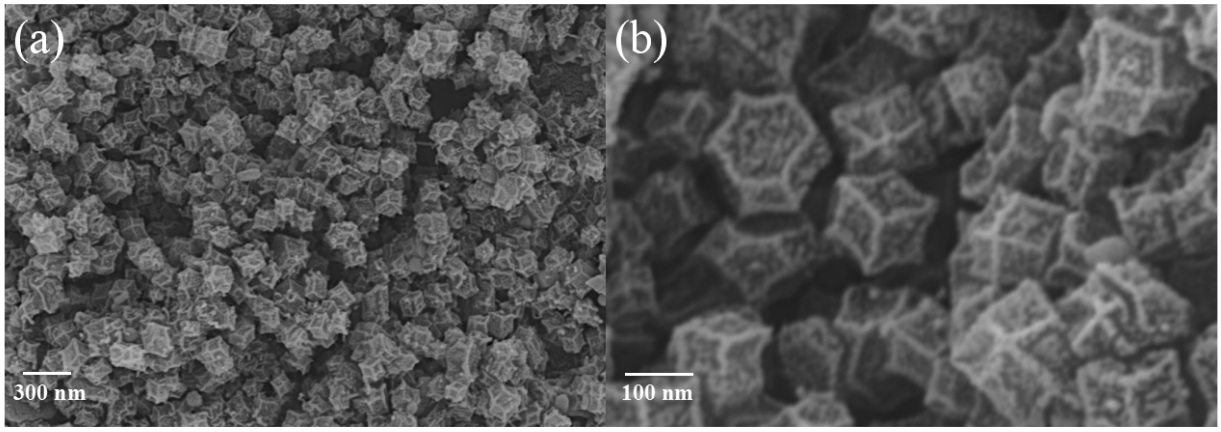

Figure S20. SEM image of Fe_2P/Co@NPC after 2000 cycles of CV test for ORR.

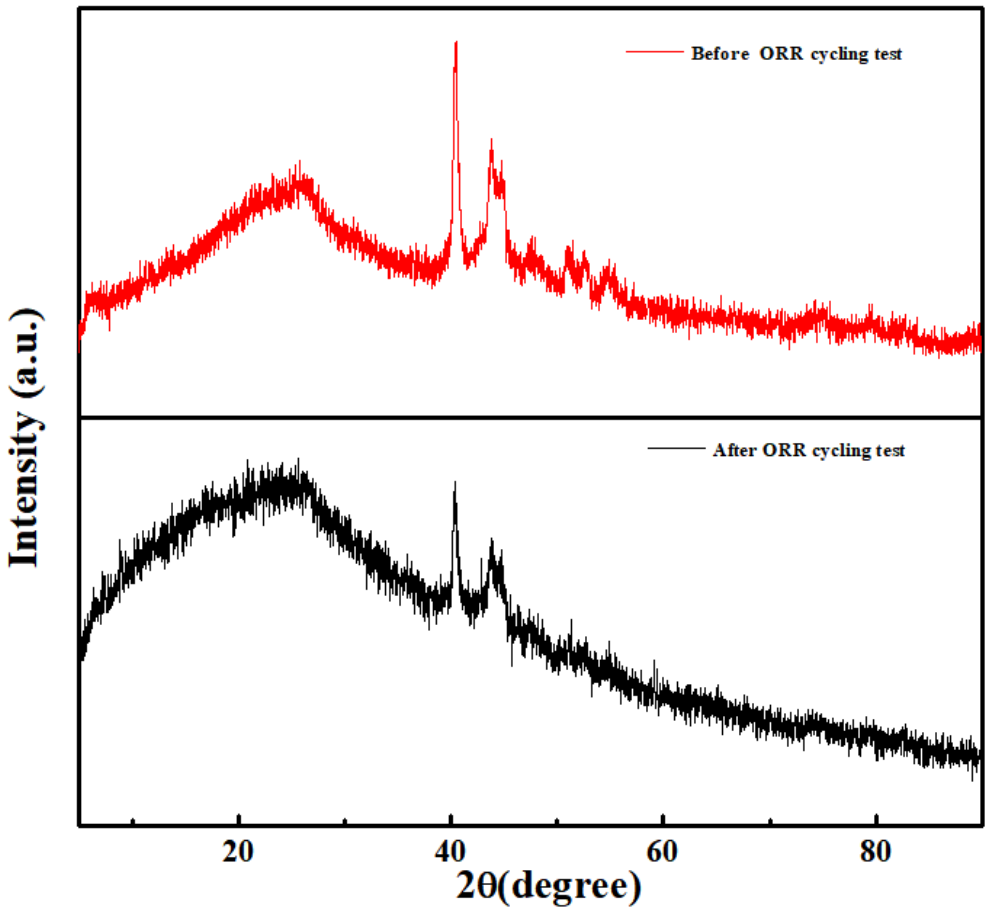

Figure S21. XRD patterns of Fe_2P/Co@NPC after 2000 cycles of CV test for ORR.

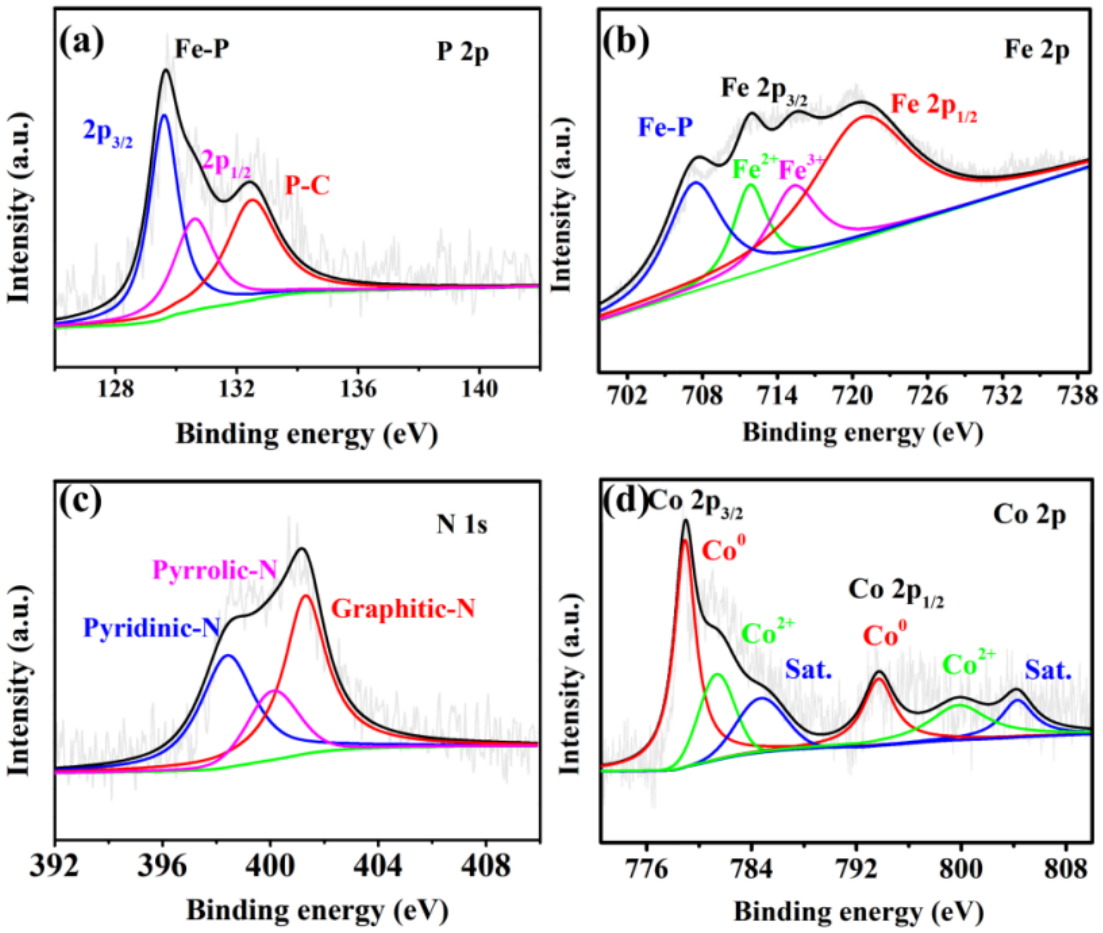

Figure S22. a) P 2p; b) Fe 2p; c) N 1s; d) Co 2p for Fe_2P/Co@NPC after 2000 cycles of CV test for ORR.

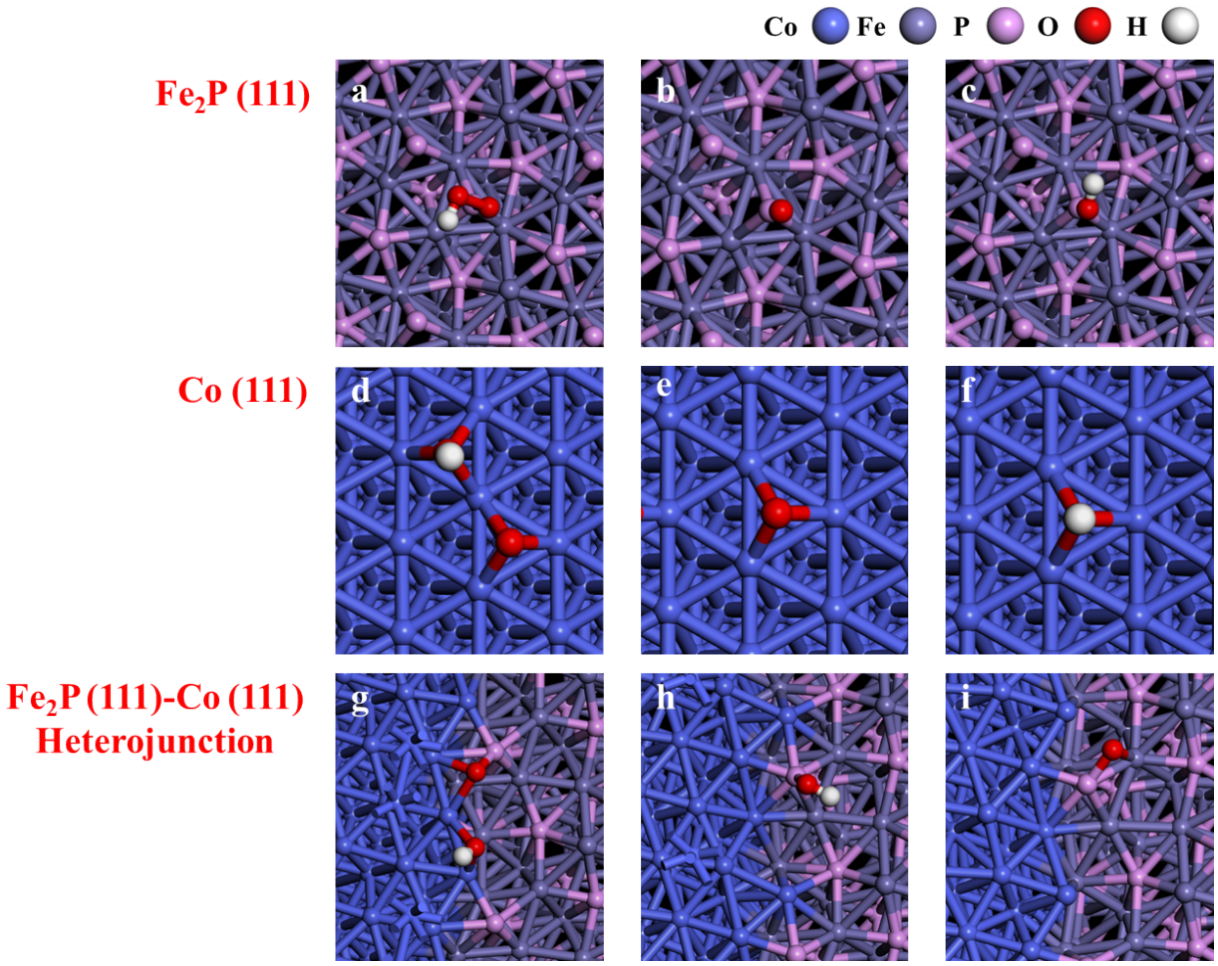

Figure S23. The three intermediates (OOH*, O*, OH*) adsorption diagram for $Fe_2P(111)$ (a-c), Co(111) (d-f), $Fe_2P(111)$-Co(111) (g-i).

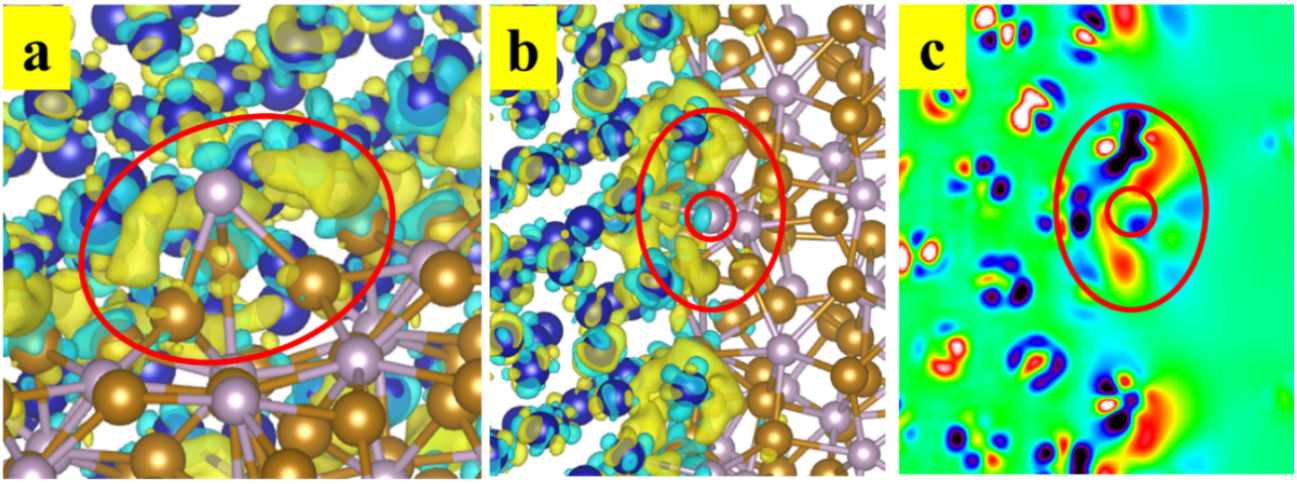

Figure S24. The Charge transfer diagram 3d (a-b) and 2d (c) at the Fe_2P(111)-Co(111) heterojunction interface represented by charge density differential method, where yellow represents charge increase and blue represents charge decrease. It can be seen that the electrons around the P active site (at the interface) are greatly increased.

Table S1. Inductively coupled plasma (ICP) results of different electrocatalysts (wt %).

Sample	Fe	Co
Co@NC	/	10.10
Fe_2P@NPC	4.95	/
Fe_2P/Co@NPC-850	5.51	2.70
Fe_2P/Co@NPC-950	6.13	5.42
Fe_2P/Co@NPC-1050	5.58	2.75

Table S2. The comparison of ORR, OER and HER activity of Fe_2P/Co@NPC with recently reported electrocatalysts.

Catalysts	ORR $E_{1/2}$ (V)	OER η_{10} (mV)	HER η_{10} (mV)	Reference
Fe_2P/Co@NPC	**0.876**	**331**	**235**	**This work**
FeCo/CO_2P@NPCF	0.770	330	260	9
Fe-N_4 SAs/NPC	0.885	430	202	10
PPy/ FeTCPP/Co	0.860	340	240	11
Fe_3C-Co/NC	0.885	340	238	12
Co-Co_9S_8@SN-CNTs-900	0.810	450	240	13
CoSA+Co_9S_8/HCNT	0.855	330	250	14
CO_2P/CoNPC	0.843	326	208	15
Co/CNFs (1000)	0.896	320	190	16
Co@N-CNTF	0.810	350	220	17

Table S3. Summary the performance of H_2/O_2 AEMFCs for non-precious metal catalysts.

Catalysts	Cathode loading (mg cm^{-2})	Anode loading (mg cm^{-2})	Pmax (mW cm^{-2})	Reference
Fe_2P/Co@NPC	**1.0**	**0.4 Pt-Ru**	**1250**	**This work**
Ce/Fe-NCNW	1.0	0.75 Pt-Ru	496	18
Fe-N-MPC	2.0	0.8 Pt-Ru	473	19
Cu SAC	2.0	0.5 Pt	196	20
NFC@Fe/Fe_3C-9	2.0	0.4 Pt	237	21
FeSiNC_50a	3.0	0.4 Pt-Ru	208	22
Fe-LC-900	2.0	0.8 Pt	50	23
NBSCP	3.0	0.4 Pt	172	24
$Fe_{0.5}$–N-C	1.0	Pt-Ru	504	25
$Co_{1.08}Fe_{3.34}$@NGT	3.0	0.4 Pt	117	26

Table S4. Summary the performance of Zn-air battery with previously reported electrocatalysts.

Catalysts	Open Voltage (V)	Pmax (mW cm^{-2})	Reference
Fe_2P/Co@NPC	**1.35**	**233.56**	**This work**
Co-NDC	1.30	154.00	27
Co-N-CNTs	1.36	101.00	1
Fe-SCNS	1.47	163.00	28
PcCu-O_8-Co/CNT	1.37	94.00	29
Fe-N/P-C-700	1.42	133.20	30
FeCo@C MS.	1.34	86.09	31
CO_2FeO_4/NCNTs	1.43	90.68	32
CoNi-SAs/NC	1.36	101.40	33

Table S5. Free energy of each intermediate process, each value has been corrected for zero-point energy and entropy (G_K) to get $\Delta\mathbf{G}$. Unit is eV.

Species	ΔG_{OH}	ΔG_{O*}	ΔG_{OOH*}
Co(111)	1.034	1.308	1.780
Fe_2P(111)	-0.196	-0.312	3.352
Fe_2P(111)-Co(111)	0.768	2.140	2.922

Reference

1. T. Wang, Z. Kou, S. Mu, J. Liu, D. He, I. S. Amiinu, W. Meng, K. Zhou, Z. Luo, S. Chaemchuen and F. Verpoort, *Adv. Funct. Mater.*, 2018, **28**, 1705048.
2. Y. Deng, B. Chi, J. Li, G. Wang, L. Zheng, X. Shi, Z. Cui, L. Du, S. Liao, K. Zang, J. Luo, Y. Hu and X. Sun, *Adv. Energy Mater.*, 2019, **9**, 1802856.
3. K. Mathew, R. Sundararaman, K. Letchworth-Weaver, T. A. Arias and R. G. Hennig, *J. Chem. Phys.,* 2014, **140**, 084106.
4. Z. Xiao, P. Sun, Z. Qiao, K. Qiao, H. Xu, S. Wang and D. Cao, *Chem. Eng. J.*, 2022, **446**, 137112.
5. Z. Niu, H. Liu, Z. Qiao, K. Qiao, P. Sun, H. Xu, S. Wang and D. Cao, *Mater. Today Energy*, 2022, **27**, 101043.
6. H. Xu, D. Cheng, D. Cao and X. C. Zeng, *Nat. Catal.* 2018, **1**, 339-348.
7. J. K. Norskov, J. Rossmeisl, A. Logadottir, L. Lindqvist, J. R. Kitchin, T. Bligaard and H. Jonsson, *J. Phys. Chem. B*, 2004, **108**, 17886-17892.
8. V. Wang, N. Xu, J. C. Liu, G. Tang and W. T. Geng, *Comput. Phys. Commun.* 2021, **267**, 108033.
9. Q. Shi, Q. Liu, Y. Ma, Z. Fang, Z. Liang, G. Shao, B. Tang, W. Yang, L. Qin and X. Fang, *Adv. Energy Mater.*, 2020, **10**, 1903854.
10. Y. Pan, S. Liu, K. Sun, X. Chen, B. Wang, K. Wu, X. Cao, W. C. Cheong, R. Shen, A. Han, Z. Chen, L. Zheng, J. Luo, Y. Lin, Y. Liu, D. Wang, Q. Peng, Q. Zhang, C. Chen and Y. Li, *Angew. Chem. Int. Ed.* , 2018, **57**, 8614-8618.
11. J. Yang, X. Wang, B. Li, L. Ma, L. Shi, Y. Xiong and H. Xu, *Adv. Funct. Mater.*, 2017, **27**, 1606497.
12. C. C. Yang, S. F. Zai, Y. T. Zhou, L. Du and Q. Jiang, *Adv. Funct. Mater.*, 2019, **29**, 1901949.
13. H. Han, Z. Bai, T. Zhang, X. Wang, X. Yang, X. Ma, Y. Zhang, L. Yang and J. Lu, *Nano Energy*, 2019, **56**, 724-732.
14. Y. Li, R. Cao, L. Li, X. Tang, T. Chu, B. Huang, K. Yuan and Y. Chen, *Small*, 2020, **16**, 1906735.
15. H. Liu, J. Guan, S. Yang, Y. Yu, R. Shao, Z. Zhang, M. Dou, F. Wang and Q. Xu, *Adv. Mater.*, 2020, **32**, 2003649.
16. Z. Yang, C. Zhao, Y. Qu, H. Zhou, F. Zhou, J. Wang, Y. Wu and Y. Li, *Adv. Mater.*, 2019, **31**, 1808043.
17. H. Guo, Q. Feng, J. Zhu, J. Xu, Q. Li, S. Liu, K. Xu, C. Zhang and T. Liu, *J. Mater. Chem. A*, 2019, **7**, 3664-3672.
18. J.-C. Li, S. Maurya, Y. S. Kim, T. Li, L. Wang, Q. Shi, D. Liu, S. Feng, Y. Lin and M. Shao, *ACS Catal.* , 2020, **10**, 2452-2458.
19. J. Lilloja, E. Kibena-Põldsepp, A. Sarapuu, M. Käärik, J. Kozlova, P. Paiste, A. Kikas, A. Treshchalov, J. Leis, A. Tamm, V. Kisand, S. Holdcroft and K. Tammeveski, *Appl. Catal. B*, 2022, **306**, 121113.
20. L. Cui, L. Cui, Z. Li, J. Zhang, H. Wang, S. Lu and Y. Xiang, *J. Mater. Chem. A*, 2019, **7**, 16690-16695.

21. M. Karuppannan, J. E. Park, H. E. Bae, Y. H. Cho and O. J. Kwon, *Nanoscale*, 2020, **12**, 2542-2554.
22. H. S. Kim, C. H. Lee, J.-H. Jang, M. S. Kang, H. Jin, K.-S. Lee, S. U. Lee, S. J. Yoo and W. C. Yoo, *J. Mater. Chem. A*, 2021, **9**, 4297-4309
23. R. Soni, S. N. Bhange and S. Kurungot, *Nanoscale*, 2019, **11**, 7893-7902.
24. D. W. Lee, J. H. Jang, I. Jang, Y. S. Kang, S. Jang, K. Y. Lee, J. H. Jang, H. J. Kim and S. J. Yoo, *Small*, 2019, **15**, 1902090.
25. S. H. Lee, J. Kim, D. Y. Chung, J. M. Yoo, H. S. Lee, M. J. Kim, B. S. Mun, S. G. Kwon, Y. E. Sung and T. Hyeon, *J. Am. Chem. Soc.*, 2019, **141**, 2035-2045.
26. S. Sultan, J. N. Tiwari, J.-H. Jang, A. M. Harzandi, F. Salehnia, S. J. Yoo and K. S. Kim, *Adv. Energy Mater.*, 2018, **8**, 1801002.
27. Z. Chen, Q. Wang, X. Zhang, Y. Lei, W. Hu, Y. Luo and Y. Wang, *Sci. Bull.*, 2018, **63**, 548-555.
28. L. Zou, C. C. Hou, Q. Wang, Y. S. Wei, Z. Liu, J. S. Qin, H. Pang and Q. Xu, *Angew. Chem. Int. Ed.* , 2020, **59**, 19627-19632.
29. H. Zhong, K. H. Ly, M. Wang, Y. Krupskaya, X. Han, J. Zhang, J. Zhang, V. Kataev, B. Buchner, I. M. Weidinger, S. Kaskel, P. Liu, M. Chen, R. Dong and X. Feng, *Angew. Chem. Int. Ed.* , 2019, **58**, 10677-10682.
30. K. Yuan, D. Lutzenkirchen-Hecht, L. Li, L. Shuai, Y. Li, R. Cao, M. Qiu, X. Zhuang, M. K. H. Leung, Y. Chen and U. Scherf, *J. Am. Chem. Soc.*, 2020, **142**, 2404-2412.
31. Y. Xu, B. Chen, J. Nie and G. Ma, *Nanoscale*, 2018, **10**, 17021-17029.
32. X. T. Wang, T. Ouyang, L. Wang, J. H. Zhong, T. Ma and Z. Q. Liu, *Angew. Chem. Int. Ed.* , 2019, **58**, 13291-13296.
33. X. Han, X. Ling, D. Yu, D. Xie, L. Li, S. Peng, C. Zhong, N. Zhao, Y. Deng and W. Hu, *Adv. Mater.*, 2019, **31**, 1905622.